F. Pourboghrat
Graduate Student.

K. A. Stelson
Associate Professor.
Productivity Center,
Department of Mechanical Engineering,
University of Minnesota,
Minneapolis, MN 55455

Pressbrake Bending in the Punch-Sheet Contact Region—Part 1: Modeling Nonuniformities

A simple model of pressbrake bending in the punch-sheet contact region is presented. The pressure and shear stress at the punch-sheet interface cause the stress distribution in the sheet to change as a function of angle. In Part 1 of this paper, a model to predict nonuniformities as a function of the geometry and the frictional conditions is presented. In Part 2, the model will be used to predict the formation of a gap between the sheet and the punch. Elastic and rigid-plastic material models of the sheet are considered, and are shown to produce remarkably similar results.

Introduction and Previous Work

Many models of pressbrake bending have been proposed. The purpose of these models is to predict major characteristics of the process (shape, springback, forming load, etc.) as a function of sheet material properties, geometry, and friction. If sufficiently accurate and simple enough for real time calculation, such a model can also be used for feedback control of the process [1, 2]. Of the previous models that are simple enough for real time calculation, all assume that conditions in the punch-sheet contact region are in a uniform state of pure bending. The purpose of this paper is to propose a simple model that predicts some of the nonuniformities in the punch contact region.

The simplest model of pressbrake bending consists of a circular region, where the punch is in contact with the sheet and rigid flanks [3–7]. The punch moment is assumed to be constant in the contact region, and the influence of the pressure and shear stresses between the punch and the sheet is neglected. Stelson [2] created a more accurate model, where the elastic and plastic deformation of the flanks is included, but in this model the punch contact region is again assumed to have constant bending moment.

The geometry of pressbrake bending is shown in Fig. 1. The flank angle, θ_b, is made up of two components: ψ_o, the angle of the sheet in contact with the punch and ϕ, the angle of the sheet in free space. The tooling geometry is completely described by the punch radius, r_p, die radius, r_d, and die half-width, L. The sheet is of thickness, t, so that the outer radius of the bend, r_o, is the sum of r_p and t. The inside radius of the portion of the sheet in free space is greater than the punch radius by an amount, δ.

A Model of the Punch-Sheet Contact Region

The approach here is to assume as a first approximation, that the tangential or hoop stress distribution is the same as found in a simple "strength of material" approach to bending—that is, the influence of the radial and shear stresses on the tangential stress will be neglected. The possibility of neutral axis shift, however, is included in the model. The assumed tangential stress-strain relationship is substituted into the equilibrium equations in cylindrical coordinates to calculate the radial and the shear stress distribution throughout the sheet wrapped around the punch. The following assumptions are made in the analysis:

(*1*) The sheet shape is circular in the punch contact region.

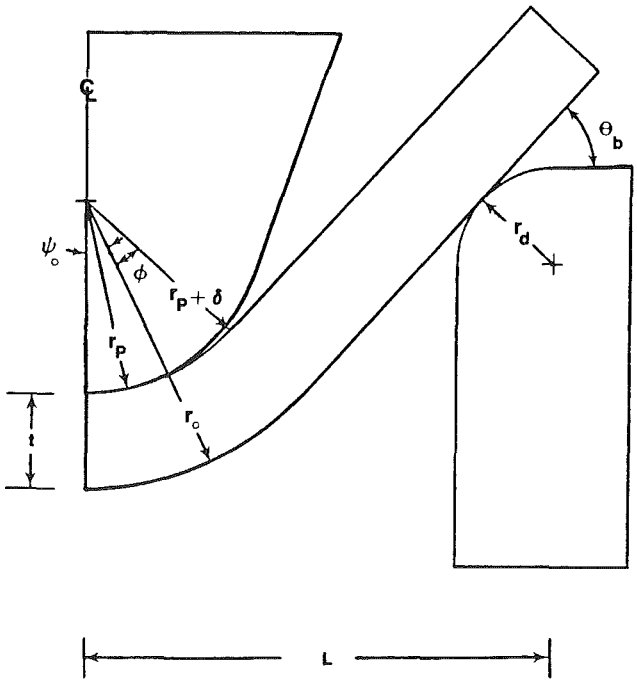

Fig. 1 The geometry of pressbrake bending

Contributed by the Production Engineering Division for publication in the JOURNAL OF ENGINEERING FOR INDUSTRY. Manuscript received at ASME Headquarters, October 30, 1987.

(2) Plane sections remain plane during bending ($e = r/r_n - 1$).
(3) The sheet thickness remains unchanged during bending.
(4) Plane strain condition is assumed since the width of the sheet in pressbrake bending is typically more than several times larger than the thickness ($e_{zz} = 0$).
(5) Radial and shear stresses have a negligible influence on the hoop stresses.
(6) The Coulomb friction assumption applies between the punch and the sheet.

Two material models are considered in the analysis: an elastic material model and a rigid-plastic material model. Of course, the elastic model is generally considered inappropriate for pressbrake bending. The model is of interest, however, if one attempts to analyze the bending of a thin strip by a large punch. Also, the elastic and rigid-plastic models are shown to produce remarkably similar results. This suggests that the analysis is insensitive to the assumed material model. It may be appropriate to use either the elastic model or the rigid-plastic model for realistic situations where significant strain hardening is present.

The equilibrium equations in cylindrical coordinates for a plane problem are:

$$\frac{\partial \tau_{r\theta}}{\partial r} + \frac{1}{r}\frac{\partial \sigma_{\theta\theta}}{\partial \theta} + 2\frac{\tau_{r\theta}}{r} = 0 \tag{1}$$

$$\frac{\partial \sigma_{rr}}{\partial r} + \frac{1}{r}\frac{\partial \tau_{r\theta}}{\partial \theta} + \frac{\sigma_{rr}}{r} - \frac{\sigma_{\theta\theta}}{r} = 0 \tag{2}$$

Elastic Material Model. The equations of elasticity for the three components of normal strain can be obtained from the generalized Hooke's law as follows:

$$e_{\theta\theta} = \frac{\sigma_{\theta\theta} - \nu(\sigma_{rr} + \sigma_{zz})}{E} \tag{3}$$

$$e_{rr} = \frac{\sigma_{rr} - \nu(\sigma_{\theta\theta} + \sigma_{zz})}{E} \tag{4}$$

$$e_{zz} = \frac{\sigma_{zz} - \nu(\sigma_{\theta\theta} + \sigma_{rr})}{E} \tag{5}$$

Assuming $e_{zz} = 0$ (plane strain) and $\sigma_{rr} = 0$ (neglecting the influence of radial stress on the hoop stress), the following relationships between $\sigma_{\theta\theta}$ and $e_{\theta\theta}$ is obtained:

$$\sigma_{\theta\theta}(r, \theta) = E' e_{\theta\theta} = E'(r/r_n - 1) \tag{6}$$

where $E' = E/(1 - \nu^2)$.

Differentiating the above expression with respect to θ gives:

$$\frac{\partial \sigma_{\theta\theta}}{\partial \theta} = E' \cdot r \cdot \frac{dK_n}{d\theta} \tag{7}$$

Substituting the above expression in the equilibrium equation in θ – direction [equation (1)] will give a first order differential equation for the shear stress, $\tau_{r\theta}$. Using the boundary condition that $\tau_{r\theta}(r_o, \theta) = 0$, that is, that the outer surface has no shear stresses, we can find the following equation for shear stresses in the wrap-around region.

$$\tau_{r\theta}(r, \theta) = \frac{E'}{3} \cdot \frac{dK_n}{d\theta} \cdot \left(\frac{r_o^3}{r^2} - r\right) \tag{8}$$

By substituting the expressions for $\sigma_{\theta\theta}$, and $\tau_{r\theta}$ into the equilibrium equation in r-direction, a first order differential equation for the radial stress, σ_{rr}, can be found. Using the boundary condition that $\sigma_{rr}(r_o, \theta) = 0$, that is, that the outer surface has no normal stress, the following equation representing the radial stress for the sheet in the wrap-around region can be found:

$$\sigma_{rr}(r, \theta) = \frac{E'}{3} \cdot \frac{d^2K_n}{d\theta^2} \cdot \left(\frac{r_o^3}{r^2} + \frac{r}{2} - \frac{3}{2}\frac{r_o^2}{r}\right) + E' \cdot \left(\frac{r}{2r_n} - 1 - \frac{r_0^2}{2rr_n} + \frac{r_o}{r}\right) \tag{9}$$

Expressions obtained for $\sigma_{\theta\theta}$, $\tau_{r\theta}$, and σ_{rr} are all functions of the neutral fiber curvature, K_n, and its derivatives with respect to θ. The Coulomb friction assumption between the punch and the sheet is:

$$\mu_p \sigma_{rr}(r_p, \theta) = \tau_{r\theta}(r_p, \theta) \tag{10}$$

Since the sheet is not slipping on the punch in most of a contact region, the use of a Coulomb friction assumption will overestimate the shear stresses. More accurate results can be obtained by using a value for the friction coefficient that is somewhat lower than the value that causes slipping. This value represents the average ratio of shear stress to pressure in the contact zone. Appropriate values for a variety of situations can be found from finite element analysis where Coulomb friction between the tooling and the sheet is included [8].

Substituting equations (8) and (9) into (10), the following second order differential equation for the neutral fiber curvature is obtained:

Nomenclature

$e_{\theta\theta}$, e_{rr}, e_{zz} = tangential, radial and z direction strain components
$\sigma_{\theta\theta}$, σ_{rr}, $\tau_{r\theta}$ = tangential, radial, and shear stresses
r_o = outside radius of the sheet
r_p, r_d = punch and die radii
r_n, K_n = radius and curvature of the neutral fiber
K_c = curvature of the center fiber
ψ_o = gap angle
ϕ = angle of free section of the sheet
θ = angular coordinate in punch-sheet contact region
$\theta_b = \psi_o + \phi$ = bend angle
F_N, F_f = normal and frictional forces at die-sheet interfaces
L_f = length of the free section of the sheet within the die
t = thickness of the sheet
$u(\ )$ = unit step function
μ = coefficient of Coulomb friction
μ_p, μ_D = punch and die coefficient of Coulomb friction
ν = Poisson ratio
E = modulus of elasticity
$E' = E/(1 - \nu^2)$
σ_Y = plane strain yield stress
$\bar{\sigma}$ = von Mises equivalent stress
M' = moment about the neutral fiber
$\sigma_{max} = E't/(2r_p + t)$
$M_o = \sigma_{max} \cdot t^2/6$, for elastic model
V_o, $T_o = \sigma_{max} \cdot t$, for elastic model
$M_o = \sigma_Y \cdot t^2/4$, for rigid-plastic model
V_o, $T_o = \sigma_Y \cdot t$, for rigid-plastic model

$$\frac{d^2K_n}{d\theta^2}+\frac{dK_n}{d\theta}\cdot\frac{2}{\mu_p}\cdot\frac{r_o^2+r_p^2+r_or_p}{(r_p-r_o)(r_p+2r_o)}+K_n\cdot 3$$
$$\cdot\frac{r_or_p+r_p^2}{(r_p-r_o)(r_p+2r_o)}-\frac{6r_p}{(r_p-r_o)(r_p+2r_o)}=0 \quad (11)$$

The solution of the differential equation is:

$$K_n(\theta)=C_1e^{s_1\theta}+C_2e^{s_2\theta}+\frac{2}{r_o+r_p} \quad (12)$$

S_1 and S_2 are the roots of the characteristic equation of equation (11), and the constants, C_1 and C_2, are calculated from the boundary conditions, which are determined from the shear and the normal forces in the sheet at the boundary between the wrap-around and the flank regions (see Appendix).

Rigid-Plastic Material Model. Taking an analogous approach for the rigid-plastic material as was taken for the elastic material, the sheet is assumed to be in a state of plane strain and the radial and shear stresses are assumed to have no influence on the hoop stress. The equation for the hoop stress becomes:

$$\sigma_{\theta\theta}(r,\theta)=-\sigma_Y+2\sigma_Yu(r-r_n) \quad (13)$$

where u is the unit step function. σ_Y is the yield stress in plane strain, which is equal to the yield stress in plane stress if the Tresca yield condition is used, and is equal to $2/\sqrt{3}$ times the yield stress in plane stress if the von Mises yield condition is used.

In the elastic bending analysis, the neutral fiber is both the unstretched fiber and the boundary between tension and compression. However, in a plastic analysis, the unstretched fiber and the boundary between tensile and compressive hoop stress are not the same. For example, Hill [9] has shown for the plane strain pure bending of a rigid-plastic material, the boundary between tensile and compressive hoop stress is at a radius equal to the geometric mean of the inner and outer radii, but the unstretched fiber is at a radius halfway between the inner and outer radii. In this paper, the term, neutral fiber, will be used to mean the boundary between tension and compression, not the unstretched fiber.

Differentiating equation (13) with respect to θ, and substituting it into the equilibrium equation in the θ-direction yields a first order differential equation for the shear stress, $\tau_{r\theta}$. Solving this equation using the boundary condition that $\tau_{r\theta}(r_o,\theta)=0$, results in the following equation for the shear stress:

$$\tau_{r\theta}(r,\theta)=2\sigma_Y\cdot\frac{dr_n}{d\theta}\cdot\frac{r_n}{r^2}\cdot[u(r-r_n)-1] \quad (14)$$

Substituting the above expressions for $\sigma_{\theta\theta}$ and $\tau_{r\theta}$ into the equilibrium equation in the radial direction results in a first order differential equation for the radial stress, σ_{rr}. Using the boundary condition that $\sigma_{rr}(r_o,\theta)=0$, the radial stress distribution can be found.

$$\sigma_{rr}(r,\theta)=\sigma_Y\left(\frac{r_o}{r}-1\right)+2\sigma_Y\left(1-\frac{r_n}{r}\right)\cdot u(r-r_n)$$
$$-2\sigma_Y\left(\frac{r_o}{r}-\frac{r_n}{r}\right)+2\sigma_Y\cdot\frac{r_n}{r^2}\cdot\frac{d^2r_n}{d\theta^2}\cdot[u(r-r_n)-1]$$
$$-2\sigma_Y\cdot\frac{1}{r}\cdot\frac{d^2r_n}{d\theta^2}\cdot[u(r-r_n)-1]$$
$$+2\sigma_Y\cdot\frac{1}{r^2}\cdot\left(\frac{dr_n}{d\theta}\right)^2\cdot[u(r-r_n)-1] \quad (15)$$

All three expressions obtained for the stresses are dependent on the radius of the neutral fiber, r_n, and its derivatives with respect to θ. Substituting into the Coulomb friction equation [equation (10)], the following nonlinear second order differential equation for the radius of the neutral fiber results:

$$\frac{d^2r_n}{d\theta^2}\cdot(r_p-r_n)-\left(\frac{dr_n}{d\theta}\right)^2+\frac{r_n}{\mu_p}\cdot\frac{dr_n}{d\theta}$$
$$+r_pr_n-\frac{1}{2}\cdot(r_or_p+r_p^2)=0 \quad (16)$$

The second order differential equation for r_n can be solved numerically using the Runge-Kutta-Nystrom method. The boundary conditions are determined from the shear and normal forces in the sheet between the wrap-around and flank regions as shown in the Appendix.

Results and Discussion

Results from using the models presented in the previous section are now presented and discussed. The following values are assumed: $\mu=0.3$, free section angle $\phi=30$ deg, $r_p/t=1$ and $L_f/t=5$. These values are typical of commerical pressbrake practice. Using this case as an example, the stress distribution, and the resulting moments and forces based on that distribution are presented. Von Mises equivalent stresses have been calculated and plotted for the rigid-plastic material to show the accuracy of neglecting the influence of shear and radial stresses on yielding.

Distribution of Moment, Curvature, Forces, and Stresses in the Punch-Sheet Contact Region. Figure 2 shows the distribution of neutral fiber curvature and moment about the neutral fiber as a function of angle for the elastic and rigid-plastic material models. The curvature is normalized by the curvature at the center of the sheet, and the moment is normalized by the bending moment with the neutral axis at the center of the sheet. As will be true of all the plots in this section, the distribution is shown at the moment of incipient gap formation (see Part 2 of the paper for a discussion of gap formation). Since the distribution is determined by boundary condition at the extreme right hand side of each plot, the distribution for smaller wrap-around angles than that plotted can be found directly from the plot by translating the axis so that the actual wrap-around angle replaces the angle of incipient gap formation at the extreme right hand side of the plot.

As can be seen from Fig. 2, the moment is not constant for either material model. The shift in neutral axis causes the moment to decrease for the elastic material and increase for the plastic material. The variations in moment, however, are extremely small, tending to validate the constant moment assumption of simpler models. This conclusion must be viewed with caution, however, since the variation in moment would be larger, if the effect of shear and radial stresses on the hoop stress were not neglected. As shown in this figure, the deviation in the position of the neutral fiber from the centerline is larger for the elastic material than the rigid-plastic material. In both cases the deviation is toward the outer surface, because of the compression in the sheet.

Figure 3 shows the variation of shear and tension forces in the wrap-around region for both material models. For the elastic case, the forces are normalized by the force resulting from a uniform stress of magnitude σ_{max} distributed across the sheet thickness, where σ_{max} is the maximum hoop stress in elastic bending when the neutral fiber lies on the centerline of the sheet. For the rigid-plastic case, the forces are normalized by the force resulting from a uniform stress of magnitude σ_y distributed across the sheet thickness. The shear force for both models is zero directly under the punch since the shear stresses vanish at this location when the gap forms (see Part 2 of the paper). As shown in this figure, a compressive force exists in the gap region after the initial gap forms, causing further separation of the sheet and punch.

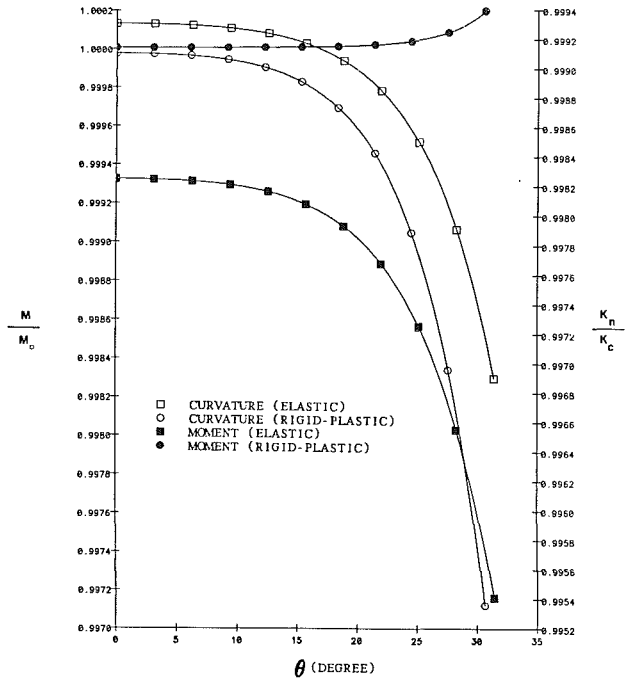

Fig. 2 Distribution of normalized moment and neutral fiber curvature in the wrap-around region for both elastic and rigid-plastic material models

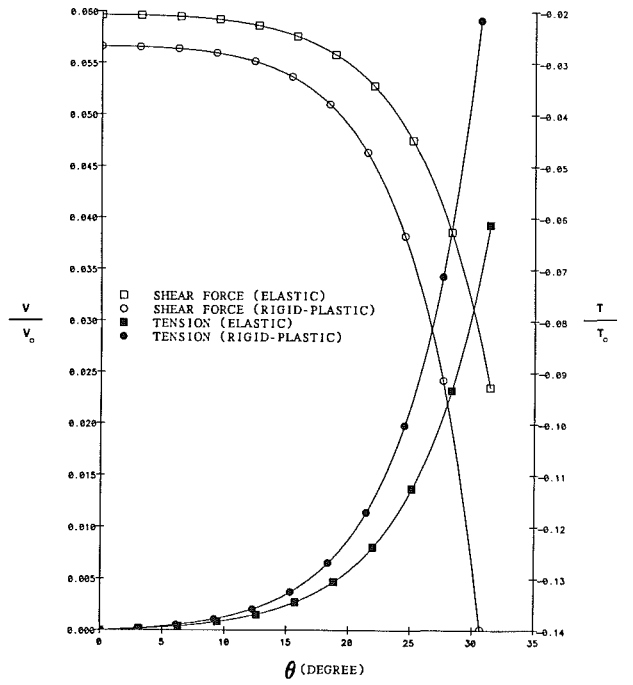

Fig. 3 Distribution of normalized shear force and tension in the wrap-around region for both elastic and rigid-plastic material models

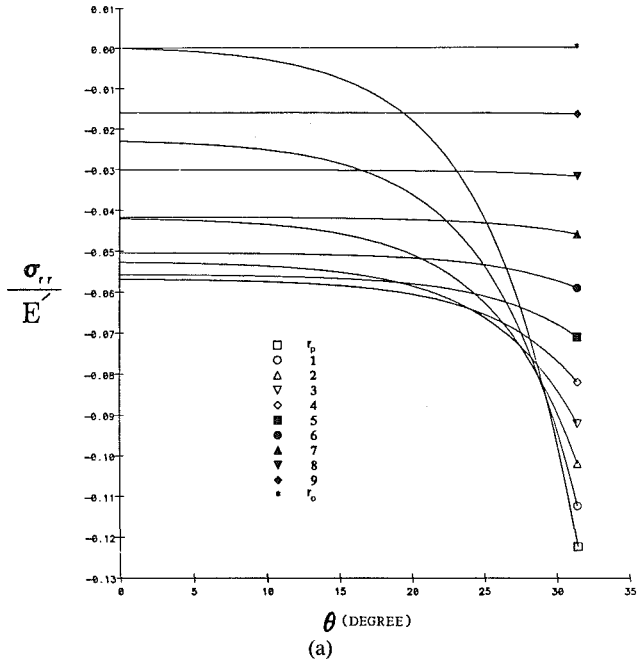

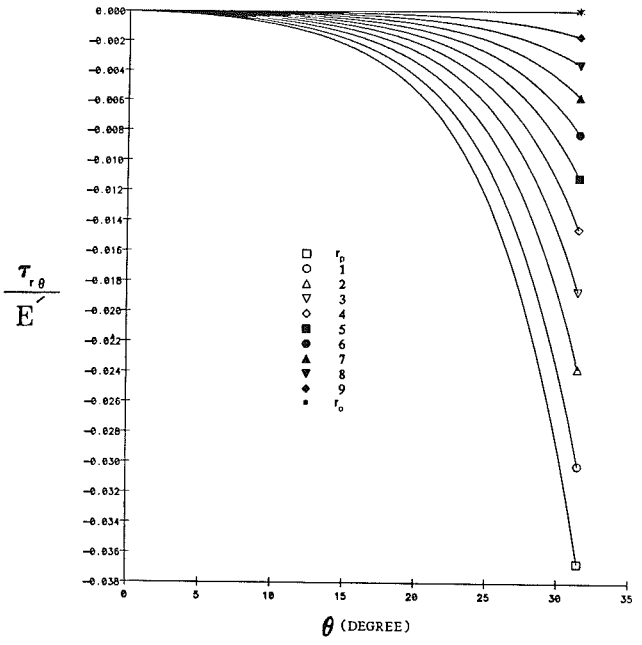

Fig. 4 Distribution of stresses for the elastic model at different radii in the wrap-around region: (*a*) radial stresses; (*b*) shear stresses

Figures 4 and 5 show the variation of radial and shear stresses for the elastic and rigid-plastic material models for various radii as a function of angle. Figures 4(*a*) and 5(*a*) show that the radial stress distribution is similar for both material models. The radial stress is negative throughout the sheet. The pressure (negative radial stress) on the outer surface is zero, and the pressure on the inner surface diminishes rapidly from its maximum value at the interface between the wrap-around region and the flanks. In the region where the pressure on the inner radius is high, the radial stress monitonically decreases in magnitude from its maximum magnitude at the inner surface to zero at the outer surface, but in the region where the pressure on the inner surface is low, the radial stress has a maximum in its magnitude near the center of the sheet.

Figures 4(*b*) and 5(*b*) show that the shear stresses for both material models are similar in the portion of the sheet in compression, but different in the portion of the sheet in tension. The rigid-plastic shear stresses become zero when the radius is greater than that of the neutral fiber [see equation (14)], while the elastic shear stresses gradually vanish as the outer surface is approached.

Figure 6 is a plot of the radial, shear, and hoop stresses for both elastic and rigid-plastic models, through the thickness of the sheet, at a section in the middle of the wrap-around region at the moment of gap formation. The hoop stress for the elastic material vanishes at the neutral fiber radius, and the

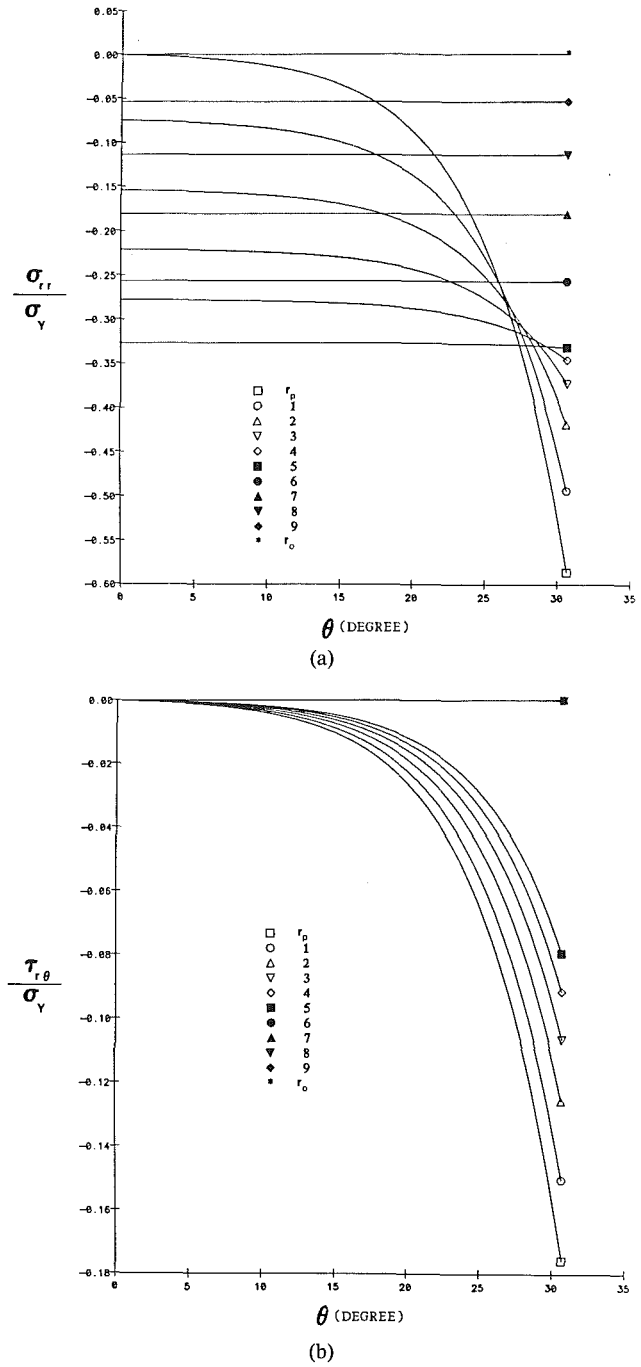

Fig. 5 Distribution of stresses for the rigid-plastic model at different radii in the wrap-around region: (*a*) radial stresses; (*b*) shear stresses

hoop stress for the rigid-plastic material jumps discontinuously from positive to negative at this point. The rigid-plastic shear stress also has a discontinuity at the neutral fiber radius. The shear stress for both models has a maximum at the inner surface. The radial stresses are at a maximum for the rigid-plastic model at the neutral fiber. This maximum is displaced toward the inner surface for the elastic model.

It is interesting to compare the stress distribution for the rigid-plastic model to the exact solution for plane strain pure bending of a rigid-plastic material [9]. Since the exact solution applies to pure bending, no shear stresses will be present. The radial stress distribution for pure bending has a similar shape to that shown in Fig. 6, being entirely compressive and having its maximum value at the neutral axis. The maximum magnitudes of the radial stress for the exact model and our approximate model are 0.346 σ_Y and 0.332 σ_Y, respectively, indicating excellent agreement even when the punch radius is equal to the thickness. In the exact solution, the hoop stress distribution is modified from its constant values on the tensile and compressive sides since the radial stress is included in the yield condition. For the exact solution with $r_p/t = 1$, the hoop stress has value of $-1.346\,\sigma_Y$ and $0.654\,\sigma_Y$ on the compressive and tensile sides of the neutral axis. This compares with the values from the approximate model of $\pm\sigma_Y$.

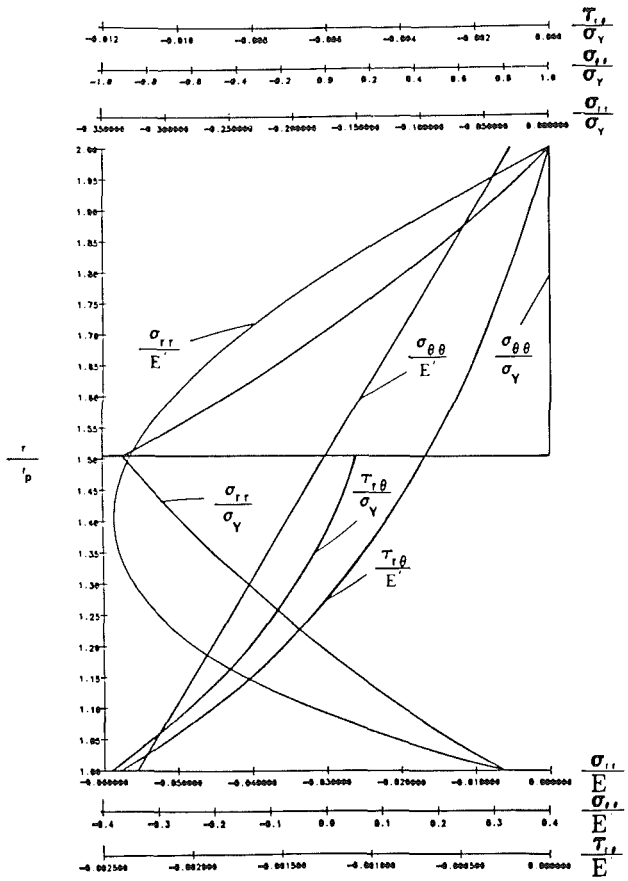

Fig. 6 Variations of hoop, radial, and shear stresses for both elastic and rigid-plastic models through the thickness of the sheet, midway in wrap-around region

Von Mises Equivalent Stress Distribution. Figure 7 shows contours of constant von Mises equivalent stress for the rigid-plastic model. If the rigid-plastic model were exact, the equivalent stress would be unity throughout, since the equivalent stress has been normalized by the yield stress. The closer the normalized von Mises equivalent stress is to unity, the more exact the approximations of the model. For Fig. 7(*a*), $r_p/t = 1$, and for Fig. 7(*b*), $r_p/t = 5$.

The model does not represent a rigid-plastic material exactly, since the effect of shear and radial stresses on the yield condition has been neglected. A comparison between Figs. 7(*a*) and 7(*b*) reveals that the approximations of the model are more exact when r_p/t is larger. Since gap formation is more common when the punch radius is much larger than the sheet thickness, the model is reasonably accurate when used to predict gap formation in these conditions. Referring to Fig. 7(*a*), it can be seen that the stresses in the approximate model are less than 70 percent of the yield stress for large region on the compressive part of the sheet. The accuracy of the model must be questioned in this regime. In contrast, referring to Fig. 7(*b*), the stresses in the approximate model are within 10 percent of the yield stress over most of the sheet. The model

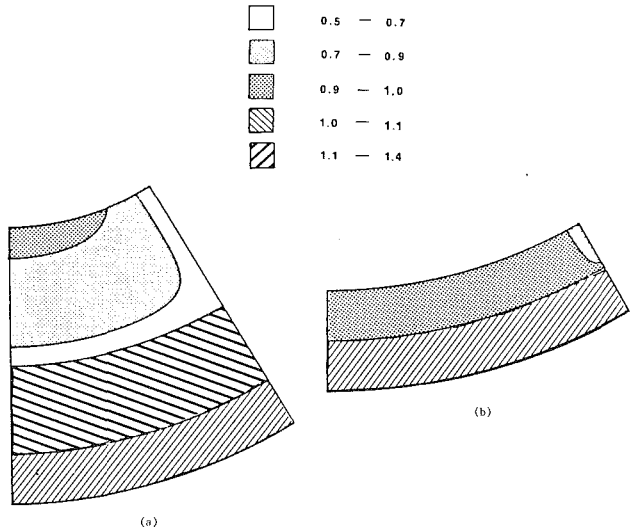

Fig. 7 Contours of constant von Mises equivalent stresses in the wrap-around region for the rigid-plastic model: (*a*) $r_p/t = 1.0$; (*b*) $r_p/t = 5.0$

also increases in accuracy as the friction coefficient between the punch and the sheet increases. This is because the higher the friction, the larger the angle over which the pressure is distributed. For the extreme case of no friction, the pressure becomes a concentrated load, and the von Mises equivalent stress becomes infinite at that point.

Conclusions

A simple model of nonuniformities in the punch-sheet region in pressbrake bending is presented. Elastic and rigid-plastic material models are considered, and found to produce similar results in most situations. This suggests that these simple models may be first approximations for more realisitic materials such as those with significant strain-hardening.

The model can be used to calculate the stress distribution in the bend and the resulting moment, tension and shear force distributions. The moment is shown to have little variation in the punch-sheet contact region. This agrees with the usual assumption of constant moment in this region. It must be noted, however, that the effects of radial and shear stresses on the hoop stress has been neglected, and the inclusion of these effects would undoubtedly increase the moment variation. Knowledge of the approximate tension and shear force distributions from the rigid-plastic model enables one to calculate the shape change on elastic unloading due to these forces.

Acknowledgments

This research was funded by contract number NSF/DMC-8451623-01 from the National Science Foundation.

References

1 Stelson, K. A., and Gossard, D. C., "An Adaptive Pressbrake Control Using an Elastic-Plastic Material Model," ASME JOURNAL OF ENGINEERING FOR INDUSTRY, Vol. 104, No. 4, Nov. 1982, pp. 389–393.

2 Stelson, K. A., "An Adaptive Pressbrake Control for Strain-Hardening Materials," ASME JOURNAL OF ENGINEERING FOR INDUSTRY, Vol. 108, No. 2, May 1986, pp. 127–132.

3 Cook, N. H., *Manufacturing Analysis*, Addison-Wesley, Reading, Mass., 1966, pp. 112–115.

4 Dannemann, E., Werkzeuggeometrie und Stemplekraft beim Biegen im V-Gesenk," *Werkstattstechnik*, Vol. 64, 1974, pp. 527–531.

5 Pawalkat, H., "Grobbleche mit grossen Radien beigen: Betrag zur Bestimmung der Beigekraefte," *Baender. Bleche. Rohre*, Vol. 16, No. 9, Sept. 1975, pp. 373–381.

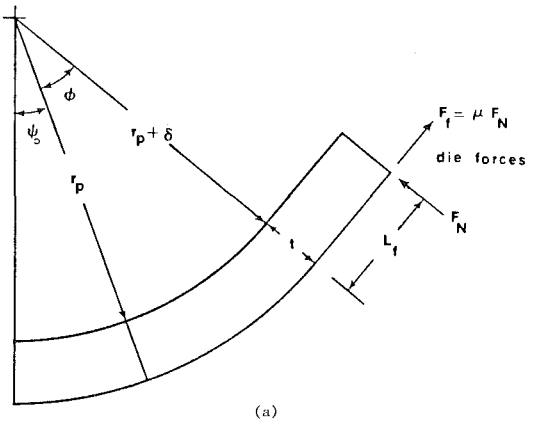

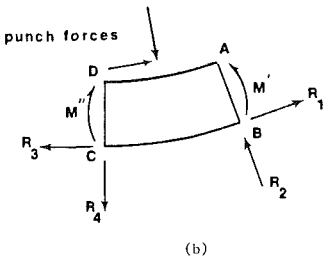

Fig. 8 Assumed sheet geometry: (*a*) overall shape; (*b*) free-body diagram of wrap-around region

6 Weinmann, K. J., and Shippell, R. J., "Effect of Tool and Workpiece Geometries upon Bending Forces and Springback in 90 deg V-die Bending of HSLA Steel Plate," *Sixth North American Metalworking Research Conference Proceedings*, May 1978, pp. 220–227.

7 White, J. B., "The Press-Bending of Rectangular Bars," *International Conference on Manufacturing Engineering*, Aug. 25–27, 1980, pp. 97–104.

8 Kim, S., and Stelson, K. A., "Finite Element Method for the Analysis and Calibration of a Closed Loop Control Algorithm for Pressbrake Bending," *1986 American Control Conference Proceedings*, June 1986, pp. 572–577.

9 Hill, R., *The Mathematical Theory of Plasticity*, Clarendon, Oxford, 1950, pp. 287–294.

APPENDIX

Boundary Conditions

The boundary conditions are derived assuming that the sheet consists of three regions: a circular region in contact with the punch, a circular region that is not in contact with the punch, and straight flanks. The assumed sheet shape is shown in Fig. 8. The circular region that is not in contact with the punch is assumed to have a radius that is infinitesimally larger than the punch radius and is used to model the finite deformation of the sheet in free space. The sheet is assumed to be moving downward against the die to establish the direction of the friction force. As will be shown in Part 2 of this paper, this assumption is usually correct. If the sheet is moving upward against the die, the following derivation is also valid with $-\mu_d$ replacing μ_d.

To solve the second order differential equations for the elastic model [equation (11)] or the rigid-plastic model [equation (16)], two boundary conditions are needed: one for the curvature or radius of curvature at the edge of the punch-sheet contact region (plane AB in Fig. 8) and one for the rate of change with respect to angle of curvature or radius of curvature at the same point. These conditions are found by equating expressions for the tension, shear, and moment at plane AB derived from the stress distribution in the sheet to

expressions for these same forces and moments in terms of the die forces exerted on the sheet.

In Fig. 8, the total bend angle, θ_b, is the sum of ψ_0 and ϕ, the wrap-around angle and the free angle. The angle, ϕ, initially increases rapidly until the sheet wraps around the punch and then remains nearly constant as the contact region between the sheet and punch grows. The reaction forces, R_1 and R_2, and the moment, M', on plane AB can be found from the normal and frictional die forces, F_N and $F_f = \mu F_N$, as follows:

$$R_1 = F_N(\mu_D \cos\phi - \sin\phi) \tag{A1}$$

$$R_2 = F_N(\cos\phi + \mu_D \sin\phi) \tag{A2}$$

$$M' = F_N[L_f + r_n \sin\phi + \mu_D(r_o - r_n \cos\phi)] \tag{A3}$$

The reactions and moment on plane AB can also be found from the stresses in the sheet as follows:

$$R_1 = \int_{r_p}^{r_o} \sigma_{\theta\theta}\, dr \tag{A4}$$

$$R_2 = -\int_{r_p}^{r_o} \tau_{r\theta}\, dr \tag{A5}$$

$$M' = \int_{r_p}^{r_o} \sigma_{\theta\theta}(r - r_n)\, dr \tag{A6}$$

Elastic Material. Equating the expressions for the reactions and moment on the plane AB found from the die forces and from the elastic stress distribution, the following three expressions are found for the normal force at the die-sheet interface:

$$F_N = \frac{E' \cdot \left(\frac{r_o^2 - r_p^2}{2r_n(\psi_o)} - r_o + r_p\right)}{(\mu_D \cos\phi - \sin\phi)} \tag{A7}$$

$$F_N = \frac{-\frac{dK_n}{d\theta}(\psi_o) \cdot \frac{E'}{3} \cdot \left(-\frac{3r_o^2}{2} + \frac{r_o^3}{r_p} + \frac{r_p^2}{2}\right)}{(\cos\theta + \mu_D \sin\phi)} \tag{A8}$$

$$F_N = \frac{E'\left[\frac{r_o^3 - r_p^3}{3r_n(\psi_o)} + (r_o - r_p)r_n(\psi_o) - (r_o^2 - r_p^2)\right]}{L_f + \mu_D r_o + (\sin\phi - \mu_D \cos\phi) r_n(\psi_o)} \tag{A9}$$

Equating equations (A7) and (A9), the following expression can be found for $K_n(\psi_0)$:

$$K_n(\psi_o) = \frac{[-3t(r_o + r_p)(\mu_D \cos\phi - \sin\phi) + 6tL_f + 6t\mu_D r_o]}{[3tL_f(r_o + r_p) + 3\mu_D t(r_o + r_p)r_o - 2(r_o^3 - r_p^3)(\mu_D \cos\phi - \sin\phi)]} \tag{A10}$$

Equating equations (A7) and (A8) the following expression can be found for $dK_n/d\theta(\psi_0)$:

$$\frac{dK_n}{d\theta}(\psi_o) = -\frac{3[(r_o + r_p)K_n(\psi_o) - 2]r_p(\cos\phi + \mu_D \sin\phi)}{t(2r_o + r_p)(\mu_D \cos\phi - \sin\phi)} \tag{A11}$$

Rigid-Plastic Material. The boundary conditions for the rigid-plastic material model can be derived using the same procedure as the elastic model. The equations for the reactions and moment on plane AB in terms of the die forces [equations (A1), (A2), and (A3)] are valid for both models. Since the stress distributions are different for the two models, the relationship between the stresses and these reactions will be different. Substituting the rigid-plastic stress distribution into equations (A4), (A5), and (A6), and equating these moments and reactions to equations (A1), (A2), and (A3) the following expressions for the normal force at the die-sheet interface are found:

$$F_N = \frac{\sigma_Y \cdot [r_o + r_p - 2r_n(\psi_o)]}{(\mu_D \cos\phi - \sin\phi)} \tag{A12}$$

$$F_N = -\frac{2\sigma_Y \cdot \left[1 - \frac{r_n(\psi_o)}{r_p}\right] \cdot \frac{dr_n}{d\theta}(\psi_o)}{(\cos\phi + \mu_D \sin\phi)} \tag{A13}$$

$$F_N = \frac{\sigma_Y \cdot \left[\frac{r_o^2}{2} + r_n^2(\psi_o) - (r_o + r_p)r_n(\psi_o)\right]}{[L_f + \mu_D r_o - (\mu_D \cos\phi - \sin\phi)r_n(\psi_o)]} \tag{A14}$$

Equating equations (A12) and (A14), the following expression for $r_n(\psi_0)$ can be found:

$$r_n(\psi_o) = \frac{L_f + \mu_D r_o}{(\mu_D \cos\phi - \sin\phi)} \pm \left\{\left[\frac{L_f + \mu_D r_o}{(\mu_D \cos\phi - \sin\phi)}\right]^2 - \frac{(r_o + r_p)(L_f + \mu_D r_o)}{(\mu_D \cos\phi - \sin\phi)} - \frac{r_o^2 + r_p^2}{2}\right\}^{1/2} \tag{A15}$$

Since $r_n(\psi_o) > 0$, the positive root of equation (A15) is taken.

Equating equations (A12) and (A13), the following expression for $dr_n/d\theta(\psi_0)$ can also be found:

$$\frac{dr_n}{d\theta}(\psi_o) = -\frac{(\cos\phi + \mu_D \sin\phi)}{(\mu_D \cos\phi - \sin\phi)} \cdot \frac{r_p(r_o + r_p - 2r_n(\psi_o))}{2(r_p - r_n(\psi_o))} \tag{A16}$$